FRONTIERS OF PHYSICS

RESEARCH ARTICLE
Volume 18 / Issue 4 / 42303 / 2023

Demonstration of fully-connected quantum communication network exploiting entangled sideband modes

Fan Li[1,*], Xiaoli Zhang[1,*], Jianbo Li[1], Jiawei Wang[1], Shaoping Shi[1,†], Long Tian[1,2], Yajun Wang[1,2], Lirong Chen[1], Yaohui Zheng[1,2,‡]

1 State Key Laboratory of Quantum Optics and Quantum Optics Devices, Institute of Opto-Electronics, Shanxi University, Taiyuan 030006, China
2 Collaborative Innovation Center of Extreme Optics, Shanxi University, Taiyuan 030006, China
Corresponding authors. E-mail: †ssp4208@sxu.edu.cn, ‡yhzheng@sxu.edu.cn
*These authors contributed equally to this work.
Received January 30, 2023; accepted February 10, 2023

ABSTRACT

Quantum communication network scales point-to-point quantum communication protocols to more than two detached parties, which would permit a wide variety of quantum communication applications. Here, we demonstrate a fully-connected quantum communication network, exploiting three pairs of Einstein–Podolsky–Rosen (EPR) entangled sideband modes, with high degree entanglement of 8.0 dB, 7.6 dB, and 7.2 dB. Each sideband modes from a squeezed field are spatially separated by demultiplexing operation, then recombining into new group according to network requirement. Each group of sideband modes are distributed to one of the parties via a single physical path, making sure each pair of parties build their own private communication links with high channel capacity better than any classical scheme.

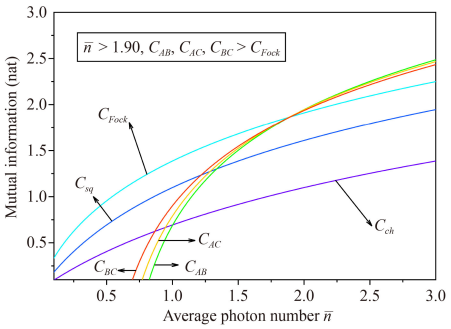

Keywords quantum network, quantum communication, entangled sideband modes, quantum dense coding

1 Introduction

The building of quantum communication networks is a central task in the field of flexible quantum information processing [1–5], including distributed quantum sensing [6–8], ultra-large scale quantum computation etc [9–11]. The simplest quantum communication schemes rely on bipartite entanglement, the entanglement of a pair of systems shared by two communicating parties. In virtue of shared entanglement, these basic quantum communication protocols that include quantum key distribution (QKD), quantum teleportation and quantum dense coding have been demonstrated in laboratory, especially QKD presented in the real world [12, 13]. Despite numerous demonstrations of point-to-point quantum communication protocols, it is faced with difficulty of scaling the standard two-party communication protocols to more than two parties under the premise of without sacrificing security, functionality and capacity, which would permit a wide variety of quantum communication applications.

To address the problem, a multitude of diverse quantum network architectures have been experimentally achieved. The first is trusted node networks [14, 15], which can be constructed by connecting bipartite quantum communication schemes with trusted nodes, forming mesh-type networks. However, there has a potential security risk from the trusted node. The second is transparent node networks [16, 17], which can be realized in configurations with passive beam splitters (or active optical switches)

Higher Education Press

https://doi.org/10.1007/s11467-023-1269-3

that establish a temporary quantum link at a time. But the secure channel capacity of each link is limited due to time-sharing configuration. The third is multi-partite (high-dimensional) entanglement based architecture [18–22], which is established by sharing entanglement state among several parties. However, in the configuration the node number is dependent how many partite is the entanglement state, making the architecture lack of flexible and scalable. The last is fully-connected networks, in which every party is directly connected to every other party by sharing bipartite entanglement between any two parties. Following the thought, fully-connected network architectures were demonstrated, exploiting a polarization-entangled photon source as quantum resource. Continuous variable (CV) physical system enjoys deterministic quantum state generation, unconditional operations and ultrahigh detection efficiencies [23–26], which represents the complementary relation with respect to discrete-variable system. However, fully-connected network architecture with more than two parties for a CV optical system remains experimentally unexplored due to challenges in implementing demultiplexing and multiplexing operation with ultra-low losses.

In the previous presentation, we demonstrated four-fold channel multiplexing point-to-point quantum communication based on CV [27], exploiting a squeezed state of light via low-loss demultiplexing operation and high-performance feedback control. Following the previous presentation, we report the demonstration of a fully-connected CV quantum dense coding communication network with high capacity of each link and low crosstalk between two links. Three pairs of entangled sideband modes from a squeezed field are spatially separated by demultiplexing operation, then recombining into new group according to network requirement, distributing to each party connected with the network. In this way, we distribute bipartite entanglement between any pairs of parties. In virtue of a frequency-comb-type control scheme, all of these ring filter cavities (as a frequency-dependent beam splitter) and relative phases operate stably at the theoretical working point, constructing general and reliable demultiplexing and multiplexing system. The demonstration opens an innovative possibility to implement more large-scale quantum communication network.

2 Experimental setup

The schematic diagram of the fully-connected quantum dense coding communication network is shown in Fig. 1. The main laser source is home-made single-frequency laser with the wavelength and output power of 1064 nm and 2 W. The laser transmits through a mode cleaner (MC) that provides spatial-temporal filtering, polarization purifying, intensity-noise and phase-noise suppressing for the downstream experiment, generating the output power of 1.6 W. Approximately 1.4 W of the output power is injected into the second harmonic generator (SHG) where the pump beam is generated for the optical

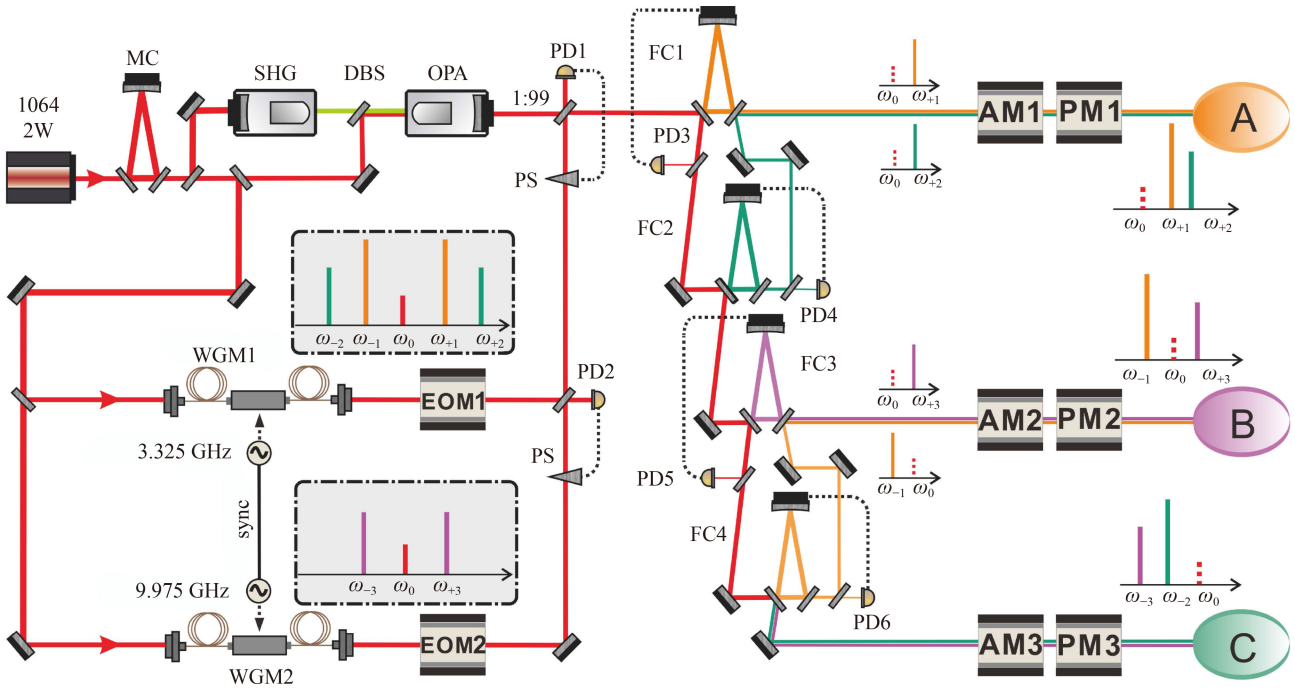

Fig. 1 Schematic of the experimental setup. MC, mode cleaner; SHG, second harmonic generator; OPA, optical parametric amplifier; FC, filter cavity; WGM, waveguide electro–optic modulator; EOM, electro–optic phase modulator; PS, phase shifter; DBS, dichroic beam splitter; PD, photodetector; AM, amplitude modulator; PM, phase modulator.

parametric amplifier (OPA) downstream. A small fraction of the output beam from the MC is split off and serves as the seed beam for OPA, auxiliary control beam generation and local oscillator generation. Utilizing an electro-optic modulator (EOM), a phase modulation signal is imprinted on the laser beam, the length of the MC and SHG is stabilized to meet the resonance condition for the laser beam via the Pound–Drever–Hall locking technique [28]. For simplicity, the control loops are omitted in Fig. 1.

Our OPA is a semi-monolithic cavity consisting of a piezo-actuated concave mirror and a periodically poled $KTiOPO_4$ (PPKTP) crystal with the dimensions of 1 mm × 2 mm × 10 mm. In order to lengthen the effective nonlinear interaction, the crystal end face has a radius of curvature of 12 mm with high reflectivity (HR) at 1064 nm and high transmission at 532 nm, thus serving as one of cavity mirror. The plane front face of the crystal has an antireflective (AR) coating for both wavelengths. We set an air gap of 27 mm length between the crystal and the concave mirror to optimize the waist size inside the crystal. The concave mirror with a radius of curvature of 30 mm has a transmissivity of 12% ± 1.5% for 1064 nm and HR for 532 nm, which is used as the output coupler. Such a design constructs a single-resonator optical cavity with high escape efficiency [29, 30]. The OPA operates at parametric deamplification state, suppressing the noise of amplitude component to below the shot noise limit (SNL). The squeezed field involves a lot of Einstein–Podolsky–Rosen (EPR) entangled modes that distribute symmetrically around the half pump frequency [31]. Each pair of EPR entangled modes have a bandwidth of approximately 70 MHz, and frequency separation between two adjacent modes of 3.325 GHz that corresponds to free spectral range of the OPA [32–34]. Therefore, in virtue of the quantum resource, a quantum communication network with high channel capacity and low crosstalk has the potential to be constructed.

A cascade of four ring filter cavities (FC) is employed as the bandpass filters to spatially separate and recombine these sideband modes. The FC consists of two plane mirrors with a transmissivity of 10% for s-polarized beam and one curved mirror with high reflectivity. In order to efficiently separate these sideband modes, the four FCs in turn have a cavity length of 165 mm, 165 mm, 190 mm and 165 mm, respectively. Four FCs in turn resonant with these sideband modes at the frequencies ω_{+1}, ω_{+2}, ω_{+3}, ω_{-1}, respectively, thus a corresponding sideband mode is transmitted from a FC, and the other sideband modes are reflected. The resonance condition of each FC is guaranteed by utilizing an active control loop, in which an auxiliary control beam is employed to extract the error signal. The auxiliary control beam that includes these coherent sidebands $\omega_{\pm1}$, $\omega_{\pm2}$, $\omega_{\pm3}$, is generated by using two synchronous waveguide electro-optic modulators (WGM1 and WGM2) with the driving frequency of 3.325 GHz and 9.975 GHz. The sideband modes ω_{+2} separated from the FC2 is coupled with ω_{+1} on the output mirror of the FC1, recombining the sideband modes ω_{+2}, ω_{+1} into a single physical path, in which the modes ω_{+2}, ω_{+1} are distributed to the party A. Similar to the previous operation, the sideband mode ω_{-3} is multiplexed with ω_{-1}, and then distributed to the party B. The remaining sideband modes ω_{-2}, ω_{-3} reflected from FC4 are routed to the party C. Each party now has two quantum channels, thus sharing a different entangled state with every other party. According to the standard technical protocol of CV quantum dense coding communication [35, 36], we encode the classical amplitude and phase signals on one half of each EPR beam respectively by electro-optic amplitude modulators (AM) and electro-optic phase modulators (PM), which represents the transmitted signals in quantum communication. The signals are decoded at the receiver with the aid of the other half of each EPR beam.

For implementing decoding operation, three pairs of local oscillators (LOs) at $\omega_{\pm1}$, $\omega_{\pm2}$, $\omega_{\pm3}$ have to be prepared as reference beam of balanced homodyne detections (BHDs). These LOs are generated by three WGMs and subsequent optical mode cleaners, which has been detailedly shown in our previous publications [27]. Each sideband mode is carefully mode matched with the corresponding frequency LO on a 50/50 beam splitter, and the output of the 50/50 beam splitter is directed toward a BHD to observe noise level. The BHDs, with the common mode rejection ratio of 75 dB [37], is built from a pair of p-i-n photodiodes (from Laser Components) with quantum efficiency of more than 99%.

3 Experimental results

Figure 2 presents the measured results of original squeezed degree with Blue line after the OPA but before the demultiplexing. The directly observed squeezing level is 12.5 dB below the SNL. To characterize the performance of the sideband entangled states after the demultiplexing and recombining operation, the measurement is performed directly without the AM and PM presenting. With the signal ports of the two BHDs blocked, the output of the joint measurement corresponds to the SNL (Black line). One of the BHD's phase keeps constant while another BHD's phase is scanned linearly in time, the spectral densities of the joint measurement are recorded. The variances of amplitude sum and phase difference are unbiased and equal to 8.0 dB for the communication link AB (Green line, $\omega_{\pm1}$), 7.6 dB for the communication link AC (Yellow line, $\omega_{\pm2}$) and 7.2 dB for the communication link BC (Red line, $\omega_{\pm3}$), respectively, without the correct of the electronic noise. According to the inseparable criteria [38] of

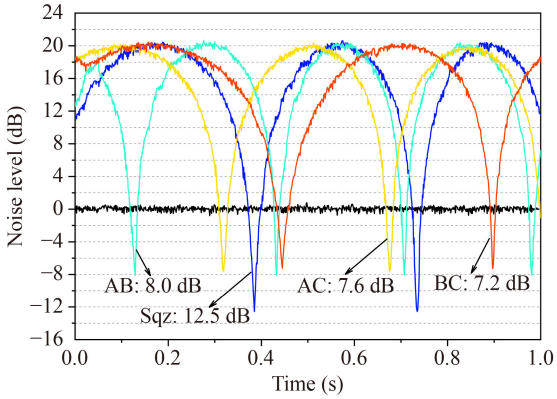

Fig. 2 Balanced homodyne measurements of the quadrature noise variances. The measurement is recorded at the analysis frequency of 2 MHz; RBW, resolution bandwidth = 300 kHz; VBW, video bandwidth = 200 Hz.

$\mathrm{Var}\left(\hat{X}_A + \hat{X}_B\right) + \mathrm{Var}\left(\hat{Y}_A - \hat{Y}_B\right) < 2$, the measured correlation variances in the left of the inequality are 0.317 for $\omega_{\pm 1}$, 0.348 for $\omega_{\pm 2}$, 0.381 for $\omega_{\pm 3}$, respectively, witnessing the presence of entanglement of these sideband modes.

Further, several AMs and PMs are placed in each communication link to simulate the transmitted signals. Without imposing modulation signal on the AMs and PMs, we record the noise power spectrum at three communication links, as shown in Fig. 3. The green line represents channel background noise of one half of the EPR beam without the help of the other half of the EPR beam. The red and blue lines are the noise spectrum of amplitude sum and phase difference, which is 7.0 dB for the communication link AB, 6.8 dB for the communication link AC, 6.5 dB for the communication link BC less than the SNL.

We simulate the transmitted signal with the intensity that exactly equals to the SNL, the signal-to noise ratios (SNRs) at different links are shown in Fig. 4. It can be

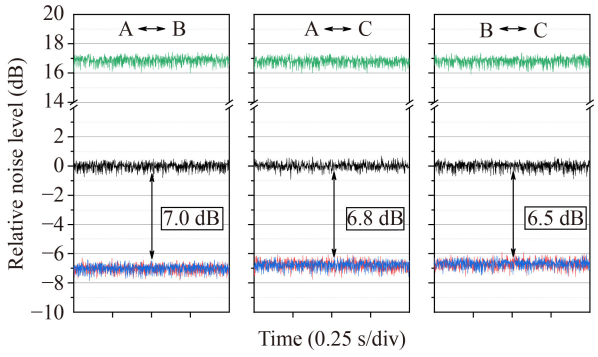

Fig. 3 Normalized quantum noise level of amplitude sum and phase difference at three communication links, corresponding to three pairs of entangled sideband modes shared by each two parties. When one half of the EPR beam is blocked, the noise spectrum is higher than the SNL.

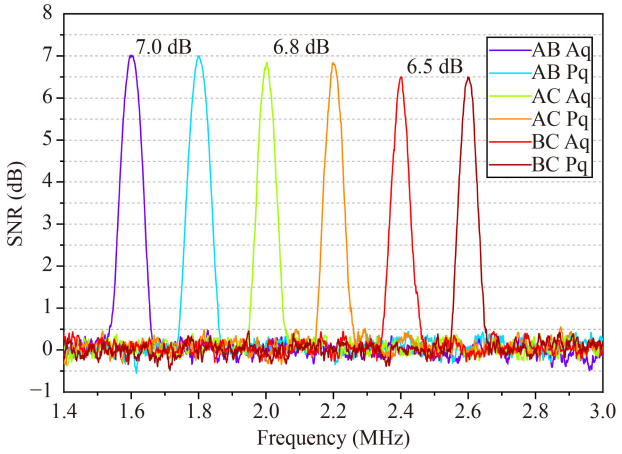

Fig. 4 Normalized SNR of each communication link based on QDC protocol. Aq, amplitude quadrature; Pq, phase quadrature.

seen that the sensitivities on both the amplitude and phase quadratures are beyond that of the SNL by means of exploiting the EPR entanglement, while the signal is submerged in the background noise without the EPR entanglement present. In order to clearly present the measurement results, we use different modulation frequency 1.6 MHz (amplitude quadrature) and 1.8 MHz (phase quadrature) at the communication link AB, 2.0 MHz (amplitude quadrature) and 2.2 MHz (phase quadrature) at the communication link AC, 2.4 MHz (amplitude quadrature) and 2.6 MHz (phase quadrature) at the communication link BC to simulate the transmitted signals, corresponding to the SNR of 7.0 dB, 6.8 dB, 6.5 dB, respectively. For each link, the SNR that retrieves the signals is equal for amplitude and phase quadratures.

According to communication theory, the signal-to noise ratio exactly is an indicator of channel capacity [39–41]. Using the above measured SNRs, we evaluate

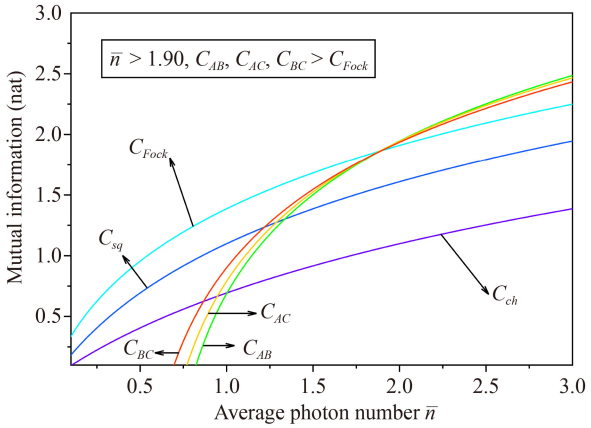

Fig. 5 Channel capacity by various channels, measured by mutual information as functions of the average photon number.

the channel capacity of each communication link at quantum dense coding communication network. Figure 5 compares the channel capacity of each link with that of other communication protocols. We can see that for communication link BC (AB), the channel capacity of the quantum dense coding communication C_{BC} (C_{AB}) has exceeded that of other CV quantum communication protocols, such as coherent state C_{ch}, squeezed state with the optimal value C_{sq}, Fock state communication C_{Fock}, which is the Holevo limit of a single-mode bosonic channel, under the condition of > 0.87 (1.01), 1.22 (1.34), 1.90 (1.90) ($\overline{n}$ stands for the average photon number), respectively [41].

In the above experiment, in order to facilitate the exhibition of the communication process between each user, the amplitude and phase quadrature are demonstrated using quantum dense coding with a small frequency difference (0.2 MHz), meanwhile employing different frequency point in each communication link. Limited by the bandwidth of OPA and FC, the bandwidth of each communication link are dozens of MHz. By expanding the bandwidth of each channel and changing the dense coding frequency, combined with other quantum communication protocols, we hope to achieve continuous variable quantum communication networks with larger communication capacity.

4 Conclusion

In conclusion, we have successfully realized a proof-of-principle demonstration of a CV quantum dense coding communication network. Any party can be connected to any other party connected with the network by their own private link, which is constructed by sharing a pair of exclusive sideband entanglement modes. Therefore, all of three parties is fully connected via sideband entanglement optical modes from one squeezed state of light. Thanks to the special auxiliary control scheme, we build the low-loss demultiplexing and multiplexing system, guaranteeing high channel capacity of each link. Since CV entanglement state is susceptible to system loss, the demultiplexing and multiplexing system with low loss is extremely important to achieve the high-performance communication network. It is worthy of noting that the scheme is easily extended to communication network with more parties, if we can combines with new technology, including the filter cavity of waveguide [42], and integrate silicon-based material [43–45]. The stable control of the entire system can be achieved through passive methods such as temperature factor, greatly reducing the difficulty and complexity, and further improve the scalability of proposed network.

Acknowledgements We acknowledge the financial support from the National Natural Science Foundation of China (NSFC) (Grant Nos. 62225504, 62027821, 62035015, U22A6003, and 12174234), the National Key R&D Program of China (Grant No. 2020YFC2200402), and the Program for Sanjin Scholar of Shanxi Province.

References

1. C. Weedbrook, S. Pirandola, R. García-Patrón, N. J. Cerf, T. C. Ralph, J. H. Shapiro, and S. Lloyd, Gaussian quantum information, *Rev. Mod. Phys.* 84(2), 621 (2012)
2. S. L. Braunstein and P. van Loock, Quantum information with continuous variables, *Rev. Mod. Phys.* 77(2), 513 (2005)
3. H. J. Kimble, The quantum internet, *Nature* 453(7198), 1023 (2008)
4. A. Furusawa and N. Takei, Quantum teleportation for continuous variables and related quantum information processing, *Phys. Rep.* 443(3), 97 (2007)
5. T. Liu, B. Q. Guo, Y. H. Zhou, J. L. Zhao, Y. L. Fang, Q. C. Wu, and C. P. Yang, Transfer of quantum entangled states between superconducting qubits and microwave field qubits, *Front. Phys.* 17(6), 61502 (2022)
6. V. Giovannetti, S. Lloyd, and L. Maccone, Advances in quantum metrology, *Nat. Photonics* 5(4), 222 (2011)
7. V. Giovannetti, S. Lloyd, and L. Maccone, Quantum metrology, *Phys. Rev. Lett.* 96(1), 010401 (2006)
8. L. Pezzè, A. Smerzi, M. K. Oberthaler, R. Schmied, and P. Treutlein, Quantum metrology with nonclassical states of atomic ensembles, *Rev. Mod. Phys.* 90(3), 035005 (2018)
9. R. Raussendorf and H. J. Briegel, A one-way quantum computer, *Phys. Rev. Lett.* 86(22), 5188 (2001)
10. S. Takeda and A. Furusawa, Toward large-scale fault-tolerant universal photonic quantum computing, *APL Photonics* 4(6), 060902 (2019)
11. B. Cheng, X. H. Deng, X. Gu, Y. He, G. C. Hu, P. H. Huang, J. Li, B. C. Lin, D. W. Lu, Y. Lu, C. D. Qiu, H. Wang, T. Xin, S. Yu, M. H. Yung, J. K. Zeng, S. Zhang, Y. P. Zhong, X. H. Peng, F. Nori, and D. P. Yu, Noisy intermediate-scale quantum computers, *Front. Phys.* 18(2), 21308 (2023)
12. H. K. Lo, M. Curty, and K. Tamaki, Secure quantum key distribution, *Nat. Photonics* 8(8), 595 (2014)
13. F. Grosshans, G. Van Assche, J. Wenger, R. Brouri, N. J. Cerf, and P. Grangier, Quantum key distribution using Gaussian-modulated coherent states, *Nature* 421, 238 (2003)
14. S. K. Liao, W. Q. Cai, J. Handsteiner, B. Liu, J. Yin, L. Zhang, D. Rauch, M. Fink, J. G. Ren, W. Y. Liu, Y. Li, Q. Shen, Y. Cao, F. Z. Li, J. F. Wang, Y. M. Huang, L. Deng, T. Xi, L. Ma, T. Hu, L. Li, N. L. Liu, F. Koidl, P. Wang, Y. A. Chen, X. B. Wang, M. Steindorfer, G. Kirchner, C. Y. Lu, R. Shu, R. Ursin, T. Scheidl, C. Z. Peng, J. Y. Wang, A. Zeilinger, and J. W. Pan, Satellite-relayed intercontinental quantum network, *Phys. Rev. Lett.* 120(3), 030501 (2018)
15. H. Y. Liu, X. H. Tian, C. Gu, P. Fan, X. Ni, R. Yang, J. N. Zhang, M. Hu, J. Guo, X. Cao, X. Hu, G. Zhao, Y. Q. Lu, Y. X. Gong, Z. Xie, and S. N. Zhu, Optical-relayed entanglement distribution using drones as

mobile nodes, *Phys. Rev. Lett.* 126(2), 020503 (2021)
16. H. Yonezawa, T. Aoki, and A. Furusawa, Demonstration of a quantum teleportation network for continuous variables, *Nature* 431(7007), 430 (2004)
17. T. Y. Chen, J. Wang, H. Liang, W. Y. Liu, Y. Liu, X. Jiang, Y. Wang, X. Wan, W. Q. Cai, L. Ju, L. K. Chen, L. J. Wang, Y. Gao, K. Chen, C. Z. Peng, Z. B. Chen, and J. W. Pan, Metropolitan all-pass and inter-city quantum communication network, *Opt. Express* 18(26), 27217 (2010)
18. W. Wang, K. Zhang, and J. T. Jing, Large-scale quantum network over 66 orbital angular momentum optical modes, *Phys. Rev. Lett.* 125(14), 140501 (2020)
19. N. Huo, Y. Liu, J. Li, L. Cui, X. Chen, R. Palivela, T. Xie, X. Li, and Z. Y. Ou, Direct temporal mode measurement for the characterization of temporally multiplexed high dimensional quantum entanglement in continuous variables, *Phys. Rev. Lett.* 124(21), 213603 (2020)
20. X. Wang, J. Fu, S. Liu, Y. Wei, and J. Jing, Self-healing of multipartite entanglement in optical quantum networks, *Optica* 9(6), 663 (2022)
21. W. Asavanant, Y. Shiozawa, S. Yokoyama, B. Charoensombutamon, H. Emura, R. N. Alexander, S. Takeda, J. Yoshikawa, N. C. Menicucci, H. Yonezawa, and A. Furusawa, Generation of time-domain-multiplexed two-dimensional cluster state, *Science* 366(6463), 373 (2019)
22. M. V. Larsen, X. Guo, C. R. Breum, J. S. Neergaard-Nielsen, and U. L. Andersen, Deterministic generation of a two-dimensional cluster state, *Science* 366(6463), 369 (2019)
23. Y. Liu, N. Huo, J. Li, and X. Li, Long-distance distribution of the telecom band intensity difference squeezing generated in a fiber optical parametric amplifier, *Opt. Lett.* 43(22), 5559 (2018)
24. Q. Zhuang, Z. Zhang, and J. H. Shapiro, Distributed quantum sensing using continuous-variable multipartite entanglement, *Phys. Rev. A* 97(3), 032329 (2018)
25. C. Oh, C. Lee, S. H. Lie, and H. Jeong, Optimal distributed quantum sensing using Gaussian states, *Phys. Rev. Res.* 2(2), 023030 (2020)
26. X. D. Wu, Y. J. Wang, H. Zhong, Q. Liao, and Y. Guo, Plug-and-play dual-phase-modulated continuous-variable quantum key distribution with photon subtraction, *Front. Phys.* 14(4), 41501 (2019)
27. S. P. Shi, L. Tian, Y. J. Wang, Y. H. Zheng, C. D. Xie, and K. C. Peng, Demonstration of channel multiplexing quantum communication exploiting entangled sideband modes, *Phys. Rev. Lett.* 125(7), 070502 (2020)
28. E. D. Black, An introduction to Pound–Drever–Hall laser frequency stabilization, *Am. J. Phys.* 69(1), 79 (2001)
29. W. H. Yang, S. P. Shi, Y. J. Wang, W. G. Ma, Y. H. Zheng, and K. C. Peng, Detection of stably bright squeezed light with the quantum noise reduction of 12.6 dB by mutually compensating the phase fluctuations, *Opt. Lett.* 42(21), 4553 (2017)
30. L. Tian, S. P. Shi, Y. H. Tian, Y. J. Wang, Y. H. Zheng, and K. C. Peng, Resource reduction for simultaneous generation of two types of continuous variable nonclassical states, *Front. Phys.* 16(2), 21502 (2021)
31. J. Roslund, R. M. de Ara'ujo, S. Jiang, C. Fabre, and N. Treps, Wavelength-multiplexed quantum networks with ultrafast frequency combs, *Nat. Photonics* 8(2), 109 (2014)
32. H. Yonezawa, S. L. Braunstein, and A. Furusawa, Experimental demonstration of quantum teleportation of broadband squeezing, *Phys. Rev. Lett.* 99(11), 110503 (2007)
33. S. Ast, A. Samblowski, M. Mehmet, S. Steinlechner, T. Eberle, and R. Schnabel, Continuous-wave nonclassical light with gigahertz squeezing bandwidth, *Opt. Lett.* 37(12), 2367 (2012)
34. S. Ast, M. Ast, M. Mehmet, and R. Schnabel, Gaussian entanglement distribution with gigahertz bandwidth, *Opt. Lett.* 41(21), 5094 (2016)
35. K. Mattle, H. Weinfurter, P. G. Kwiat, and A. Zeilinger, Dense coding in experimental quantum communication, *Phys. Rev. Lett.* 76(25), 4656 (1996)
36. S. L. Braunstein and H. J. Kimble, Dense coding for continuous variables, *Phys. Rev. A* 61(4), 042302 (2000)
37. X. L. Jin, J. Su, Y. H. Zheng, C. Y. Chen, W. Z. Wang, and K. C. Peng, Balanced homodyne detection with high common mode rejection ratio based on parameter compensation of two arbitrary photodiodes, *Opt. Express* 23(18), 23859 (2015)
38. L. M. Duan, G. Giedke, J. I. Cirac, and P. Zoller, Inseparability criterion for continuous variable systems, *Phys. Rev. Lett.* 84(12), 2722 (2000)
39. J. T. Jing, J. Zhang, Y. Yan, F. G. Zhao, C. D. Xie, and K. C. Peng, Experimental demonstration of tripartite entanglement and controlled dense coding for continuous variables, *Phys. Rev. Lett.* 90(16), 167903 (2003)
40. S. Yokoyama, R. Ukai, S. C. Armstrong, C. Sornphiphatphong, T. Kaji, S. Suzuki, J. Yoshikawa, H. Yonezawa, N. C. Menicucci, and A. Furusawa, Ultra-large-scale continuous-variable cluster states multiplexed in the time domain, *Nat. Photonics* 7(12), 982 (2013)
41. J. Mizuno, K. Wakui, A. Furusawa, and M. Sasaki, Experimental demonstration of entanglement-assisted coding using a two-mode squeezed vacuum state, *Phys. Rev. A* 71(1), 012304 (2005)
42. M. Stefszky, R. Ricken, C. Eigner, V. Quiring, H. Herrmann, and C. Silberhorn, Waveguide cavity resonator as a source of optical squeezing, *Phys. Rev. Appl.* 7(4), 044026 (2017)
43. A. Dutt, S. Miller, K. Luke, J. Cardenas, A. L. Gaeta, P. Nussenzveig, and M. Lipson, Tunable squeezing using coupled ring resonators on a silicon nitride chip, *Opt. Lett.* 41(2), 223 (2016)
44. J. S. Levy, A. Gondarenko, M. A. Foster, A. C. Turner-Foster, A. L. Gaeta, and M. Lipson, CMOS-compatible multiple-wavelength oscillator for on-chip optical interconnects, *Nat. Photonics* 4(1), 37 (2010)
45. G. Masada, K. Miyata, A. Politi, T. Hashimoto, J. L. O' Brien, and A. Furusawa, Continuous-variable entanglement on a chip, *Nat. Photonics* 9(5), 316 (2015)